
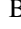




Topological surface states host superconductivity induced by the bulk condensate in YRuB₂Nikhlesh S. Mehta ¹, Bikash Patra ², Mona Garg,¹ Ghulam Mohmad,¹ Mohd Monish,¹ Pooja Bhardwaj ¹, P. K. Meena,³ K. Motla,³ Ravi P. Singh,³ Bahadur Singh,² and Goutam Sheet ^{1,*}¹*Department of Physical Sciences, Indian Institute of Science Education and Research (IISER) Mohali, Sector 81, S. A. S. Nagar, Manauli 140306, India*²*Department of Condensed Matter Physics and Materials Science, Tata Institute of Fundamental Research, Mumbai 400005, India*³*Department of Physics, Indian Institute of Science Education and Research Bhopal, Bhopal 462066, India*

(Received 15 September 2023; revised 30 January 2024; accepted 17 May 2024; published 5 June 2024)

While the possibility of topological superconductivity (TSC) in hybrid heterostructures involving topologically nontrivial band structure and superconductors has been proposed, the realization of TSC in a single stoichiometric material is most desired for fundamental experimental investigation of TSC and its device applications. Bulk measurements on YRuB₂ detect a single superconducting gap of ~ 1 meV. This is supported by our electronic structure calculations, which also reveal the existence of topological surface states in the system. We performed surface-sensitive Andreev reflection spectroscopy on YRuB₂ and detected the bulk superconducting gap as well as another superconducting gap of ~ 0.5 meV. From our analysis of electronic structure, we show that the smaller gap is formed in the topological surface states in YRuB₂ due to the proximity of the bulk superconducting condensate. Thus, in agreement with the past theoretical predictions, we present YRuB₂ as a unique system that hosts superconducting topological surface states.

DOI: [10.1103/PhysRevB.109.L241104](https://doi.org/10.1103/PhysRevB.109.L241104)

Due to the particle-hole symmetry in superconductors, the positive and negative energy eigenstates of the Bogoliubov–de Gennes Hamiltonian appear pair-wise [1]. When the superconducting condensate forms, the negative-energy eigenstates remain fully occupied. This closely resembles to the insulators where the valence band remains filled. Therefore, distinct topological invariants for the occupied states can be calculated [2–5]. A nonzero topological invariant leads to a so-called topological superconductor. In strong topological superconductors, the nonzero topological invariants may exist even when the bulk of the superconductor is fully gapped [6–8]. Due to the constraints enforced by topology, the surface of the strong topological superconductors host gapless modes, the so-called Majorana zero modes. Such systems have recently attracted enormous attention due to their fascinating properties and their potential as a key ingredient of fault-tolerant quantum computing [9–11]. Therefore, it is extremely important to search for candidate topological superconductors (TSCs).

Fu and Kane had proposed a scheme to obtain $p_x + ip_y$ type topological superconductivity induced in the topological surface states (TSSs) of a topological insulator (TI) through proximity effect, or by doping [12]. Experimentally, proximity induced superconductivity was observed in heterostructures

of superconducting NbSe₂, and BSCCO with the topological insulator Bi₂Se₃ [13,14]. Bi₂Se₃ was intercalated with metal ions like Cu [15], Nb [16], Sr [17], etc. in a controlled way to achieve superconductivity. Similarly, upon In doping, the topological crystalline insulator SnTe displayed superconductivity [18]. In all such cases, the intrinsic features of a TSC may undergo modification due to complex interface effects, strains developing from lattice mismatched heterostructures or the intercalates acting as disorder. All such issues can be overcome only if a TSC phase is realized in a single stoichiometric material system. In such a system, the Majorana zero modes may appear as exotic surface states, or as bound states in the vortex cores. As per the theoretical argument presented in [19], a TSS with a reasonably high T_c is required to experimentally resolve the Majorana bound states. However, till date, all the stoichiometric topological systems that have shown superconductivity have rather low T_c {e.g., the Dirac semimetal PdTe₂ ($T_c = 1.7$ K) [20], the nodal-line semimetal PbTaSe₂ ($T_c = 3.8$ K) [21], BiPd ($T_c = 3.8$ K) [22,23]}.

Recently, based on electronic structure calculations [19], it was proposed that the rare-earth transition-metal ternary boride YRuB₂ ($T_c = 7.6$ K) is a ideal topological superconductor candidate where all the key requirements for being a topological superconductor (namely, a relatively higher T_c , topological surface states, s -wave superconductivity, and good separation between bulk and surface states) are satisfied. In addition to the above, the calculations also suggest the existence of symmetry-protected Dirac nodal rings in YRuB₂ [24]. Motivated by such theoretical observations, we have employed Andreev reflection spectroscopy [25,26] experiments on YRuB₂. Andreev reflection spectroscopy is known to be a potentially powerful technique to probe transport through

*Also at S. N. Bose National Center for Basic Sciences, Salt Lake, JD Block, Sector III, Bidhannagar, Kolkata, West Bengal 700106, India; Present address: Materials Science Division, Argonne National Laboratory, Lemont, Illinois 60439, USA; goutam@iisermohali.ac.in

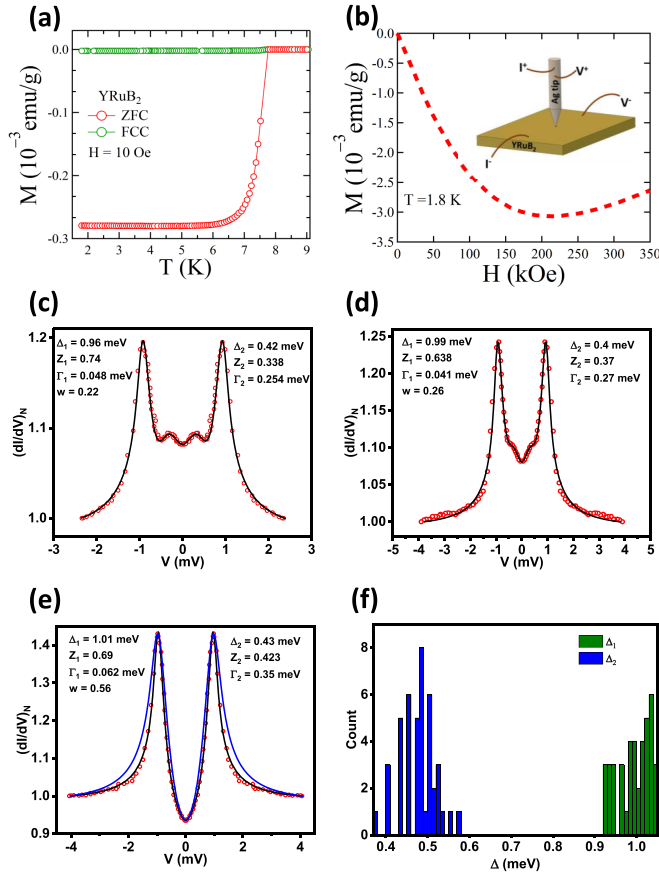


FIG. 1. (a) Temperature dependence of bulk magnetization measured in both zero-field cooling (ZFC) and field-cooled cooling mode with 10 Oe magnetic field (FCC). (b) Field dependence of bulk magnetization at a temperature of 1.8 K. Inset shows a schematic describing the formation of point contact on YRuB₂. (c),(d) Conductance spectra obtained in the ballistic regime (red circles) and their corresponding two-gap BTK fit (black line). (e) Conductance spectra obtained in the ballistic regime (red circles) and their corresponding single gap BTK fit (blue line) and two gap fit (black line). (f) Statistics of superconducting energy gaps (Δ_1 and Δ_2) for 43 different contacts.

topological surface states in a topological superconductor [27–29].

The measurements reported here were performed on polycrystalline YRuB₂ where multiple single crystallites with randomly oriented facets coexist on the surface. Temperature dependence of bulk magnetization on polycrystalline YRuB₂ in zero-field cooled (ZFC) and field-cooled cooling (FCC) mode with an applied field of 10 Oe confirm the bulk nature of superconductivity in YRuB₂ and it shows a superconducting transition onset at 7.8 K as shown in Fig. 1(a). The Andreev reflection spectroscopic measurements were performed by measuring the transport characteristics of several ballistic point contacts between superconducting YRuB₂ and normal metallic Ag tips respectively.

The electronic transport between a normal metal and a superconductor through a ballistic point contact is dominated by a process called Andreev reflection [25] that causes an enhancement of the differential conductance (dI/dV) when the

electron energy is less than the superconducting energy gap (Δ). A dI/dV vs energy ($E = eV$) spectrum thus obtained is analyzed by a modified Blonder-Tinkham-Klapwijk (BTK) model [30]. This model assumes the interface between a normal metal and a superconductor as a delta potential barrier whose strength is defined by a dimensionless parameter Z . With a small potential barrier present at the interface, two peaks symmetric about $V = 0$ appear. Such peaks are the hallmark signatures of Andreev Reflection. In Figs. 1(c)–1(e), three representative point-contact Andreev reflection (PCAR) spectra between YRuB₂ and Ag probed at $T \sim 0.45$ K are shown (red circles). All the spectra were first normalized with respect to the conductance at high bias. In all these spectra, Andreev peaks symmetric about $V = 0$, are clearly seen. No extra (anomalous) features like conductance dips [31,32] are present. This confirms that the point contacts are close to the ballistic regime of transport where true spectroscopic parameters can be obtained. We have performed such experiments at a large number of points (see Figs. S9–S12 within the Supplemental Material, SM [33]). The normal state resistance of these points varied from 0.6 Ω to 20 Ω and the contact diameters (calculated using Wexler’s formula [44]) varied between 4 nm and 24 nm. As shown in Figs. 1(c) and 1(d), there are two well-resolved peaks for both positive and negative V in the point-contact spectra obtained on YRuB₂. This is strikingly similar to the Andreev reflection spectra obtained on the two-band superconductor MgB₂ [45,46]. The solid-black lines in Figs. 1(c) and 1(d) represent the theoretical fits using the modified BTK theory generalized to include two superconducting gaps (Δ_1 and Δ_2) by writing the normalized conductance as $(\frac{dI}{dV})_N = w(\frac{dI}{dV})_{1N} + (1-w)(\frac{dI}{dV})_{2N}$, where w is the relative contribution of one of the gaps (say, Δ_1) [45]. As shown in Fig. 1(e), for certain point contacts, we also obtained spectra in which two gaps are not visually resolved. We noted that while a conventional single-gap model is insufficient to explain these spectra, the two-gap model provides a better fit to the spectra over the entire energy range. We thus obtained a distribution of the two gaps measured at different points on the surface of YRuB₂ and plotted the distribution in Fig. 1(f). As it is evident from the distribution, two prominent superconducting gaps are measured with $\Delta_1 = 0.99 \pm 0.07$ meV and $\Delta_2 = 0.47 \pm 0.1$ meV.

The above observation substantially differs from the earlier measurements of the superconducting energy gap in YRuB₂ based on bulk measurement techniques like NMR relaxation and μ -SR experiments in the past [47,48]. Both these experiments revealed one clean, fully formed superconducting gap in YRuB₂ with an amplitude of ~ 1.1 meV that followed BCS behavior [49]. In our experiments, the measured larger gap (Δ_1) is comparable to the bulk gap amplitude reported by the other bulk-sensitive experiments [47,48]. To understand the origin of the smaller gap (Δ_2) in our measurements, we have performed detailed first-principles calculations. We presented the calculated bulk band structure of YRuB₂ without spin-orbit coupling (SOC) in Fig. 2(a). It manifests a metallic ground state where electron and hole bands dip into each other in such a way that they form coexisting electron and hole pockets at the Fermi level. Figure 2(b) shows the calculated Fermi surface that reveals two hole pockets (light blue and teal colors) and two electron pockets (green and brown colors),

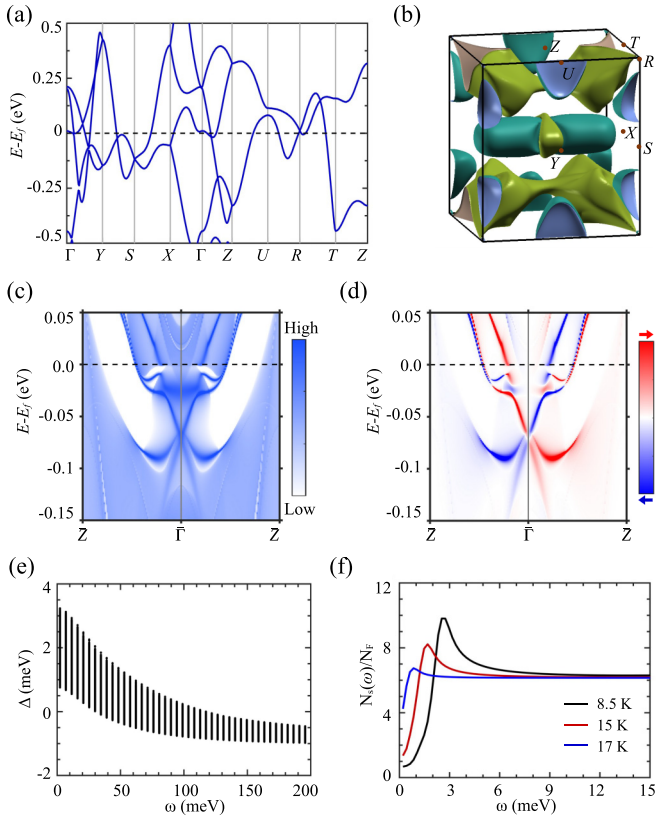


FIG. 2. (a) Calculated bulk band structure of YRuB₂ without SOC along the high-symmetry path in the Brillouin zone (BZ). (b) The associated Fermi surface with coexisting electrons (green and brown colors) and hole pockets (light blue and teal colors). (c) The (010) surface band structure along $\bar{Z} - \bar{\Gamma} - \bar{Z}$ directions. (d) The associated spin texture with up (red) and down (blue) spin polarizations. (e) Superconducting gap along the imaginary axis at $T = 8.5$ K and (f) the quasiparticle superconducting density of states (DOS) at 8.5 K, 15 K, and 17 K.

where a single superconducting gap forms (please also see SM for additional details [33]). Since YRuB₂ has nonsymmorphic symmetries, its metallic state is robust and realizes hourglass Dirac fermions at the zone boundary in the presence of SOC. Regardless, there is a band inversion between the valence and conduction bands at the Γ point such that the valence and conduction bands are separated at $k_y = 0$ plane. Such a gapped state can facilitate the calculations of Z_2 number on these planes similar to insulators. Based on the parity eigenvalues of the occupied states, we obtained a nontrivial $Z_2 = 1$ on the $k_y = 0$ plane. Figure 2(c) shows the calculated (010) surface states and associated spin texture in Fig. 2(d). These results reveal an odd number of spin-momentum-locked nontrivial states crossings along $\bar{\Gamma} - \bar{Z}$ at the Fermi level. Such nontrivial states can in principle become superconducting through the bulk proximity effect. Since point-contact spectroscopy is a more surface sensitive technique, the Andreev reflection processes in our experiments are bound to involve the bulk gap as well as the proximity induced gap in the TSSs. As a consequence, we have effectively measured two gaps in YRuB₂. We also computed the phonon dispersion and Eliashberg spectral function $\alpha^2F(\omega)$ to get the superconducting T_c (see Fig. S2

within the SM [33]). The calculated value of T_c using the McMillan formula as modified by Allen and Dynes [50] is 8.7 K. Figure 2(e) shows the superconducting gap function at 8.5 K obtained by solving the (anisotropic) Eliashberg equation along the imaginary axis. Quasiparticle density of states $N_s(\omega)/N(E_F) = \text{Re}[\omega/\sqrt{\omega^2 - \Delta^2(\omega)}]$, where $N(E_F)$ is the normal density of states (DOS) at the Fermi level, in the superconducting state is shown in Fig. 2(f). A single peak in the quasiparticle DOS signifies the presence of only a single bulk superconducting gap. The peak in the DOS gradually disappeared above 17 K. This overestimated temperature scale might be due to the possible anharmonic effects [51], or the use of an isotropic Coulomb parameter [52]. Nevertheless, considering the possibility of only one bulk superconducting gap, it is rational to surmise that the second gap measured by our experiments is a proximity-induced gap in the surface states.

Now it is important to investigate the nature of the two superconducting gaps. For that, we have investigated the response of the PCAR spectra and the corresponding Δ_1 and Δ_2 with changing temperature and magnetic fields. Figure 3(a) depicts the temperature dependence of dI/dV vs V spectra. The colored circles represent the experimentally registered data points and the solid-black lines represent the BTK fits generalized to the case of two gaps for each spectrum. For two gap fitting, the value of the weight factor w was kept fixed over the entire temperature range. At low temperatures, the position of the Andreev reflection driven peaks does not show a noticeable change. With increasing temperature, the peaks slowly broaden and eventually all spectral features disappear at a temperature of 7.6 K, near the critical temperature of the superconductor. Figure 3(b) shows the temperature dependence of Δ_1 and Δ_2 extracted from the spectrum shown in Fig. 3(a). Here, the red and green dots represent the extracted values of Δ_1 and Δ_2 respectively and the solid-black lines represent the expected temperature dependence of Δ_1 and Δ_2 for a conventional BCS superconductor [49]. Good quality BTK fits of the experimental data and a near-BCS temperature dependence of both the gaps show that the corresponding order parameters are conventional in nature. The extracted value of Δ_{01} and Δ_{02} for this particular spectrum are 0.97 meV and 0.43 meV respectively. The corresponding $\frac{2\Delta_0}{k_B T_c}$ for Δ_1 and Δ_2 were found to be ~ 2.96 and 1.32 respectively. The ratio corresponding to the larger gap falls within the weak-coupling BCS regime and is consistent with the previous bulk-sensitive experiments [47,48]. The temperature dependence of a representative spectrum of the other type where the two gaps are not visually resolved, along with the respective theoretical fits within the two-gap model, is also shown in Fig. 3(c). The two gaps extracted from this point also follows the BCS temperature dependence as shown in Fig. 3(d).

In order to obtain additional understanding on the two gaps of YRuB₂, we performed magnetic field dependence of the PCAR spectra. Figure 3(e) shows the magnetic field dependence of dI/dV vs V spectra. The colored circles represent the experimentally obtained spectra and the solid black lines represent the two gap BTK fits for each spectrum. With increasing magnetic field, Andreev reflection driven conductance peaks close smoothly and all the superconductivity-related features disappear at a magnetic

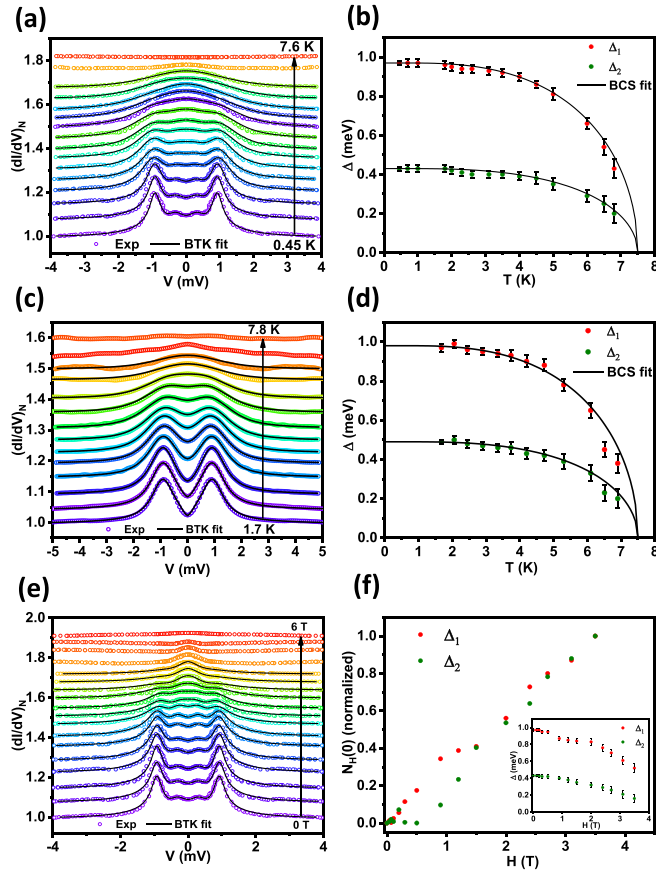


FIG. 3. (a) Temperature (T) dependence of the conductance spectra (colored circles) with two gap BTK fit (black line). (b) Variation of the two superconducting gaps (Δ_1 and Δ_2) with temperature (T). (c) T dependence of the conductance spectra of other type where two gaps are not visually resolved. (d) Evolution of Δ_1 and Δ_2 , extracted from the spectra shown in Fig. 3(c), with T . (e) Magnetic field (H) dependence of the conductance spectra (colored circles) with two gap BTK fit (black line) at 0.45 K. (f) H dependence of zero bias density of states ($N_H(0)$) after subtracting the zero field contribution corresponding to Δ_1 and Δ_2 . The *inset* shows the variation of the two superconducting gaps (Δ_1 and Δ_2) with H .

field of ~ 6 T. The extracted value of Δ_1 and Δ_2 for the spectra at zero magnetic field and at a temperature of 0.45 K are 0.97 meV and 0.43 meV respectively. The variation of Δ_1 and Δ_2 with the magnetic field are shown in inset of Fig. 3(f). For lower magnetic fields (upto 2 T) Δ_1 and Δ_2 do not change significantly and they decrease smoothly with further increasing magnetic field. Beyond this field, Δ_1 and Δ_2 fall rapidly and a linear extrapolation of data shows that Δ_2 has a tendency to disappear at a magnetic field of ~ 4.8 T, while Δ_1 at ~ 5.8 T.

In the context of the conventional multiband superconductor MgB_2 , it was earlier shown that the zero bias density of states (DOS) corresponding to the smaller gap grows far more rapidly and attains the normal state value much before that corresponding to the larger gap [53]. We have calculated the zero-bias density of states (DOS) using the Dyne's

formula given as $N(E) = \text{Re}[\frac{E-i\Gamma}{\sqrt{(E-i\Gamma)^2-\Delta^2}}]$ [54]. Magnetic field dependence of $N(0)$ corresponding to Δ_1 and Δ_2 for the spectra shown in Fig. 3(e) is shown in Fig. S13 within the SM [33]. Figure 3(f) shows the corresponding field dependence of $N_H(0) = N(0) - N_0(0)$ where N_0 is the zero-bias DOS for $H = 0$. For YRuB_2 , it appears that the effect of magnetic field on the DOS corresponding to both the larger and the smaller gap is the same and they evolve with field following a similar trend. This suggests that the two gaps do not independently form in two different bands, but are closely related where the smaller gap is induced in the TSS by the larger one in the bulk. Within this picture, since the amplitude of the proximity-induced gap varies between the crystallite facets, the relatively large distribution of the measured superconducting energy gaps is understood as a consequence of the randomly oriented crystallite facets on the surface of our sample on which the Ag tip falls.

In conclusion, we have performed point-contact Andreev reflection spectroscopy experiments on the candidate topological superconductor YRuB_2 . Although based on bulk measurements, YRuB_2 is thought to be a single-gap superconductor, in our experiments we detected multiple superconducting gaps centered around two amplitudes, 0.99 meV and 0.47 meV. We have shown through the first-principles calculations that the emergence of the smaller gap in our surface sensitive experiments is a consequence of a proximity induced superconducting gap in the TSSs in the system, some of which cross the Fermi surface and contribute in global transport. The properties of the larger gap is consistent with that probed by bulk-sensitive experiments. Therefore, our experiments show that YRuB_2 is a potentially important superconductor where the interaction between topological surface states and bulk superconductivity leads to novel physical insights in understanding the candidate topological superconductors.

We acknowledge SEM Central Facility at IISER Mohali. N.S.M. thanks University Grants Commission (UGC) Government of India for senior research fellowship (SRF). G.M. thanks UGC for junior research fellowship (JRF). M.G. thanks the Council of Scientific and Industrial Research (CSIR), Government of India, for financial support through a research fellowship [Award No. 09/947(0227)/2019-EMR-I]. M.M. thanks the Council of Scientific and Industrial Research (CSIR), Government of India, for financial support through a research fellowship [Award No. 09/0947(12989)/2021-EMR-I]. We thank Sougata Mardanya for fruitful discussions in calculating the superconducting properties. We would like to thank Ms. Savita and Dr. Y. Singh for their help with resistivity measurement. The work at TIFR Mumbai was supported by the Department of Atomic Energy of the Government of India under Project No. 12-R&D-TFR-5.10-0100 and benefited from the computational resources of TIFR Mumbai. R.P.S. acknowledge the Science and Engineering Research Board, Government of India, for the Core Research Grant No. CRG/2019/001028. G.S. acknowledges financial assistance from the Science and Engineering Research Board (SERB), Govt. of India (Grant No. CRG/2021/006395).

- [1] J. Alicea, New directions in the pursuit of Majorana fermions in solid state systems, *Rep. Prog. Phys.* **75**, 076501 (2012).
- [2] C. L. Kane and E. J. Mele, Z_2 topological order and the quantum spin Hall effect, *Phys. Rev. Lett.* **95**, 146802 (2005).
- [3] L. Fu and C. L. Kane, Topological insulators with inversion symmetry, *Phys. Rev. B* **76**, 045302 (2007).
- [4] M. Z. Hasan and C. L. Kane, *Colloquium*: Topological insulators, *Rev. Mod. Phys.* **82**, 3045 (2010).
- [5] J. E. Moore and L. Balents, Topological invariants of time-reversal-invariant band structures, *Phys. Rev. B* **75**, 121306(R) (2007).
- [6] M. Sato and Y. Ando, Topological superconductors: A review, *Rep. Prog. Phys.* **80**, 076501 (2017).
- [7] X.-L. Qi and S.-C. Zhang, Topological insulators and superconductors, *Rev. Mod. Phys.* **83**, 1057 (2011).
- [8] A. P. Schnyder, S. Ryu, A. Furusaki, and A. W. W. Ludwig, Classification of topological insulators and superconductors in three spatial dimensions, *Phys. Rev. B* **78**, 195125 (2008).
- [9] C. Nayak, S. H. Simon, A. Stern, M. Freedman, and S. Das Sarma, Non-Abelian anyons and topological quantum computation, *Rev. Mod. Phys.* **80**, 1083 (2008).
- [10] S. Das Sarma, M. Freedman, and C. Nayak, Topological quantum computation, *Phys. Today* **59**, 32 (2006).
- [11] S. Das Sarma, M. Freedman, and C. Nayak, Majorana zero modes and topological quantum computation, *npj Quantum Inf.* **1**, 15001 (2015).
- [12] L. Fu and C. L. Kane, Superconducting proximity effect and Majorana fermions at the surface of a topological insulator, *Phys. Rev. Lett.* **100**, 096407 (2008).
- [13] M.-X. Wang, C. Liu, J.-P. Xu, F. Yang, L. Miao, M.-Y. Yao, C. L. Gao, C. Shen, X. Ma, X. Chen *et al.*, The coexistence of superconductivity and topological order in the Bi_2Se_3 thin films, *Science* **336**, 52 (2012).
- [14] E. Wang, H. Ding, A. V. Fedorov, W. Yao, Z. Li, Y.-F. Lv, K. Zhao, L.-G. Zhang, Z. Xu, J. Schneeloch *et al.*, Fully gapped topological surface states in Bi_2Se_3 films induced by a d -wave high-temperature superconductor, *Nat. Phys.* **9**, 621 (2013).
- [15] L. A. Wray, S.-Y. Xu, Y. Xia, Y. San Hor, D. Qian, A. V. Fedorov, H. Lin, A. Bansil, R. J. Cava, and M. Z. Hasan, Observation of topological order in a superconducting doped topological insulator, *Nat. Phys.* **6**, 855 (2010).
- [16] T. Asaba, B. J. Lawson, C. Tinsman, L. Chen, P. Corbae, G. Li, Y. Qiu, Y. S. Hor, L. Fu, and L. Li, Rotational symmetry breaking in a trigonal superconductor Nb-doped Bi_2Se_3 , *Phys. Rev. X* **7**, 011009 (2017).
- [17] Z. Liu, X. Yao, J. Shao, M. Zuo, L. Pi, S. Tan, C. Zhang, and Y. Zhang, Superconductivity with topological surface state in $\text{Sr}_x\text{Bi}_2\text{Se}_3$, *J. Am. Chem. Soc.* **137**, 10512 (2015).
- [18] S. Sasaki, Z. Ren, A. A. Taskin, K. Segawa, L. Fu, and Y. Ando, Odd-parity pairing and topological superconductivity in a strongly spin-orbit coupled semiconductor, *Phys. Rev. Lett.* **109**, 217004 (2012).
- [19] Y. Gao, P.-J. Guo, K. Liu, and Z.-Y. Lu, RRuB_2 ($R = \text{Y, Lu}$), topological superconductor candidates with hourglass-type Dirac ring, *Phys. Rev. B* **102**, 115137 (2020).
- [20] H.-J. Noh, J. Jeong, E.-J. Cho, K. Kim, B. I. Min, and B.-G. Park, Experimental realization of type-II Dirac fermions in a PdTe_2 superconductor, *Phys. Rev. Lett.* **119**, 016401 (2017).
- [21] T.-R. Chang, P.-J. Chen, G. Bian, S.-M. Huang, H. Zheng, T. Neupert, R. Sankar, S.-Y. Xu, I. Belopolski, G. Chang, B. K. Wang, F. Chou, A. Bansil, H.-T. Jeng, H. Lin, and M. Z. Hasan, Topological Dirac surface states and superconducting pairing correlations in PbTaSe_2 , *Phys. Rev. B* **93**, 245130 (2016).
- [22] Z. Sun, M. Enayat, A. Maldonado, C. Lithgow, E. Yelland, D. C. Peets, A. Yaresko, A. P. Schnyder, and P. Wahl, Dirac surface states and nature of superconductivity in Noncentrosymmetric BiPd , *Nat. Commun.* **6**, 6633 (2015).
- [23] M. Mondal, B. Joshi, S. Kumar, A. Kamlapure, S. C. Ganguli, A. Thamizhavel, S. S. Mandal, S. Ramakrishnan, and P. Raychaudhuri, Andreev bound state and multiple energy gaps in the noncentrosymmetric superconductor BiPd , *Phys. Rev. B* **86**, 094520 (2012).
- [24] In this context we also note that preliminary scanning tunnelling spectroscopy (STS) data are also consistent with the idea of topological surface states in YRuB_2 (see Fig. S3 within the SM [33]). The discrepancy in the energy scale of the surface states between theory and experiments might be due to extrinsic disorders like chemical inhomogeneities etc., that are not considered in these calculations.
- [25] A. F. Andreev, The thermal conductivity of the intermediate state in superconductors, *Zh. Eksp. Teor. Fiz.* **46**, 1823 (1964) [*Sov. Phys. JETP* **19**, 1288 (1964)].
- [26] Y. G. Naidyuk and I. K. Yanson, *Point-Contact Spectroscopy* (Springer, Berlin, 2005).
- [27] S. Sasaki, M. Kriener, K. Segawa, K. Yada, Y. Tanaka, M. Sato, and Y. Ando, Topological superconductivity in $\text{Cu}_x\text{Bi}_2\text{Se}_3$, *Phys. Rev. Lett.* **107**, 217001 (2011).
- [28] H. Peng, D. De, B. Lv, F. Wei, and C.-W. Chu, Absence of zero-energy surface bound states in $\text{Cu}_x\text{Bi}_2\text{Se}_3$ studied via Andreev reflection spectroscopy, *Phys. Rev. B* **88**, 024515 (2013).
- [29] W. Dai, A. Richardella, R. Du, W. Zhao, X. Liu, C. X. Liu, S.-H. Huang, R. Sankar, F. Chou, N. Samarth, and Q. Li, Proximity-effect-induced superconducting gap in topological surface states—A point contact spectroscopy study of $\text{NbSe}_2/\text{Bi}_2\text{Se}_3$ superconductor-topological insulator heterostructures, *Sci. Rep.* **7**, 7631 (2017).
- [30] G. E. Blonder, M. Tinkham, and T. M. Klapwijk, Transition from metallic to tunneling regimes in superconducting microconstrictions: Excess current, charge imbalance, and supercurrent conversion, *Phys. Rev. B* **25**, 4515 (1982).
- [31] G. Sheet, S. Mukhopadhyay, and P. Raychaudhuri, Role of critical current on the point-contact Andreev reflection spectra between a normal metal and a superconductor, *Phys. Rev. B* **69**, 134507 (2004).
- [32] R. Kumar and G. Sheet, Nonballistic transport characteristics of superconducting point contacts, *Phys. Rev. B* **104**, 094525 (2021).
- [33] See Supplemental Material at <http://link.aps.org/supplemental/10.1103/PhysRevB.109.L241104> for methods, experimental details, analysis of PCAR spectra, estimation of point contact diameter, phonon dispersion and Eliashberg spectral function calculations, scanning tunnelling microscopy/spectroscopy data, scanning electron microscopy data, resistivity data and additional data, which also includes Refs. [30,34–43,45,50].
- [34] S. Das and G. Sheet, A modular point contact spectroscopy probe for sub-Kelvin applications, *Rev. Sci. Instrum.* **90**, 103903 (2019).
- [35] P. Giannozzi, O. Andreussi, T. Brumme, O. Bunau, M. B. Nardelli, M. Calandra, R. Car, C. Cavazzoni, D. Ceresoli,

- M. Cococcioni *et al.*, Advanced capabilities for materials modelling with quantum ESPRESSO, *J. Phys.: Condens. Matter* **29**, 465901 (2017).
- [36] N. Troullier and J. Luís, Efficient pseudopotentials for plane-wave calculations, *Phys. Rev. B* **43**, 1993 (1991).
- [37] M. J. van Setten, M. Giantomassi, E. Bousquet, M. J. Verstraete, D. R. Hamann, X. Gonze, and G.-M. Rignanese, The PseudoDojo: Training and grading a 85 element optimized norm-conserving pseudopotential table, *Comput. Phys. Commun.* **226**, 39 (2018).
- [38] D. M. Ceperley and B. J. Alder, Ground state of the electron gas by a stochastic method, *Phys. Rev. Lett.* **45**, 566 (1980).
- [39] J. P. Perdew and A. Zunger, Self-interaction correction to density-functional approximations for many-electron systems, *Phys. Rev. B* **23**, 5048 (1981).
- [40] F. Giustino, M. L. Cohen, and S. G. Louie, Electron-phonon interaction using Wannier functions, *Phys. Rev. B* **76**, 165108 (2007).
- [41] S. Poncé, E. R. Margine, C. Verdi, and F. Giustino, EPW: Electron-phonon coupling, transport and superconducting properties using maximally localized Wannier functions, *Comput. Phys. Commun.* **209**, 116 (2016).
- [42] A. Pleceník, M. Grajcar, Š. Beňačka, P. Seidel, and A. Pfuch, Finite-quasiparticle-lifetime effects in the differential conductance of $\text{Bi}_2\text{Sr}_2\text{CaCu}_2\text{O}_y/\text{Au}$ junctions, *Phys. Rev. B* **49**, 10016 (1994).
- [43] E. R. Margine and F. Giustino, Anisotropic Migdal-Eliashberg theory using Wannier functions, *Phys. Rev. B* **87**, 024505 (2013).
- [44] G. Wexler, The size effect and the non-local Boltzmann transport equation in orifice and disk geometry, *Proc. Phys. Soc.* **89**, 927 (1966).
- [45] R. S. Gonnelli, D. Daghero, G. A. Ummarino, V. A. Stepanov, J. Jun, S. M. Kazakov, and J. Karpinski, Direct evidence for two-band superconductivity in MgB_2 single crystals from directional point-contact spectroscopy in magnetic fields, *Phys. Rev. Lett.* **89**, 247004 (2002).
- [46] P. Szabó, P. Samuely, J. Ka Kačmarčík, T. Klein, J. Marcus, D. Fruchart, S. Miraglia, C. Marcenat, and A. G. M. Jansen, Evidence for two superconducting energy gaps in MgB_2 by point-contact spectroscopy, *Phys. Rev. Lett.* **87**, 137005 (2001).
- [47] Y. Kishimoto, Y. Kawasaki, Y. Ideta, S. Endou, T. Tanaka, M. Tanabe, T. Ohno, G. Ghosh, A. K. Tyagi, and L. C. Gupta, ^{11}B NMR study on rare earth ternary borides RRuB_2 , *J. Phys.: Conf. Ser.* **176**, 012039 (2009).
- [48] J. A. T. Barker, R. P. Singh, A. D. Hillier, and D. McK. Paul, Probing the superconducting ground state of the rare-earth ternary boride superconductors RRuB_2 ($R = \text{Lu}, \text{Y}$) using muon-spin rotation and relaxation, *Phys. Rev. B* **97**, 094506 (2018).
- [49] J. Bardeen, L. N. Cooper, and J. R. Schrieffer, Theory of superconductivity, *Phys. Rev.* **108**, 1175 (1957).
- [50] P. B. Allen and R. C. Dynes, Transition temperature of strongly-coupled superconductors reanalyzed, *Phys. Rev. B* **12**, 905 (1975).
- [51] A. Floris, G. Profeta, N. N. Lathiotakis, M. Lüders, M. A. L. Marques, C. Franchini, E. K. U. Gross, A. Continenza, and S. Massidda, Superconducting properties of MgB_2 from first principles, *Phys. Rev. Lett.* **94**, 037004 (2005).
- [52] H. J. Choi, D. Roundy, H. Sun, M. L. Cohen, and S. G. Louie, First-principles calculation of the superconducting transition in MgB_2 within the anisotropic Eliashberg formalism, *Phys. Rev. B* **66**, 020513(R) (2002).
- [53] A. E. Koshelev and A. A. Golubov, Mixed state of a dirty two-band superconductor: Application to MgB_2 , *Phys. Rev. Lett.* **90**, 177002 (2003).
- [54] R. C. Dynes, V. Narayanamurti, and J. P. Garno, Direct measurement of quasiparticle-lifetime broadening in a strongly-coupled superconductor, *Phys. Rev. Lett.* **41**, 1509 (1978).